The CO oxidation kinetics on supported Pd model catalysts: A molecular beam/*in situ* time-resolved infrared reflection absorption spectroscopy study

J. Libuda,[a] I. Meusel, J. Hoffmann, and J. Hartmann
Fritz-Haber-Institut der Max-Planck-Gesellschaft, Faradayweg 4-6, D-14195 Berlin, Germany

L. Piccolo[b] and C. R. Henry
CRMC2-CNRS, Campus de Luminy, Case 913, F-13288 Marseille Cedex 9, France

H.-J. Freund
Fritz-Haber-Institut der Max-Planck-Gesellschaft, Faradayweg 4-6, D-14195 Berlin, Germany and CRMC2-CNRS, Campus de Luminy, Case 913, F-13288 Marseille Cedex 9, France

Combining molecular beam techniques and time-resolved infrared reflection absorption spectroscopy (TR-IRAS) we have studied the kinetics of the CO oxidation reaction on an alumina-supported Pd model catalyst. The Pd particles are deposited by metal evaporation under ultrahigh vacuum (UHV) conditions onto a well-ordered alumina film, prepared on a NiAl(110) single crystal. Particle size, density and structure of the Pd deposits have been characterized in previous studies. In the low temperature region, transient and steady-state experiments have been performed over a wide range of CO and oxygen fluxes by crossing two effusive molecular beams on the sample surface. We determine the steady-state CO_2 production rate as a function of the CO fraction in the impinging gas flux. Simultaneously, the occupation of CO adsorption sites under steady-state conditions is monitored by *in situ* IR spectroscopy. The origin of different types of CO_2 transients is discussed. In particular we focus on the transient CO_2 production after switching off the CO beam. For the model catalyst investigated, detailed reaction rate measurements in combination with time-resolved IRAS show that the origin of the particular transient behavior of the supported model system is not due to the presence of specific adsorption sites on small particles, as has been proposed previously. Instead, we show that the transient behavior can be semiquantitatively simulated on the basis of a simple kinetic model considering a homogeneous surface, and accounting for the inhibition of the dissociative adsorption of O_2 at high CO coverage. Moreover, it is discussed how the inherent heterogeneity of the supported particle system can additionally enhance the observed effect. © *2001 American Institute of Physics.* [DOI: 10.1063/1.1342240]

I. INTRODUCTION

What is the molecular origin of the kinetics of heterogeneously catalyzed reactions on supported metal systems being in many cases drastically different from the corresponding single crystal surfaces? As possible answers to this fundamental question in catalysis a number of concepts have been proposed. Among these are size effects, which may alter the electronic properties of small metal particles[1,2] and thus the adsorption properties, geometrical effects due to the presence of specific adsorption sites or the combination of adsorption sites (see, e.g., Refs. 3–7), the influence of boundary sites at the metal oxide interface,[8] metal support interactions,[9–11] or support effects involving spillover from/to or reaction on the support (see, e.g., Refs. 4, 12, 13, and references therein). Recently, Zhdanov and Kasemo have pointed out that there might be a substantial influence

on the kinetics due to the coupling between nonequivalent adsorption sites by diffusion.[5–7] The presence of such nonequivalent sites such as different facets, edge, defect or particle boundary sites is an inherent property of complex catalysts which cannot be modeled in studies on simple single crystal surfaces.

In spite of the numerous concepts, specific examples are scarce where there is clear experimental evidence concerning the origin of the effects mentioned before. The reasons for this lack of detailed knowledge is connected to what is usually referred to as the ''materials gap'' between surface science and catalysis (see, e.g., Refs. 14, 15). Real catalysts are usually hardly accessible by surface science methods. Moreover, their vast complexity may preclude an assignment of kinetic effects to specific molecular features of the system. On the other hand, the mentioned effects may not be present on simple single crystals, but only on such complex surfaces.

As a possible solution to this materials problem, a variety of supported model catalysts have been developed. These models allow us to introduce certain aspects of a real catalyst in a well controlled fashion, while still maintaining the experimental accessibility. Supported model catalysts have
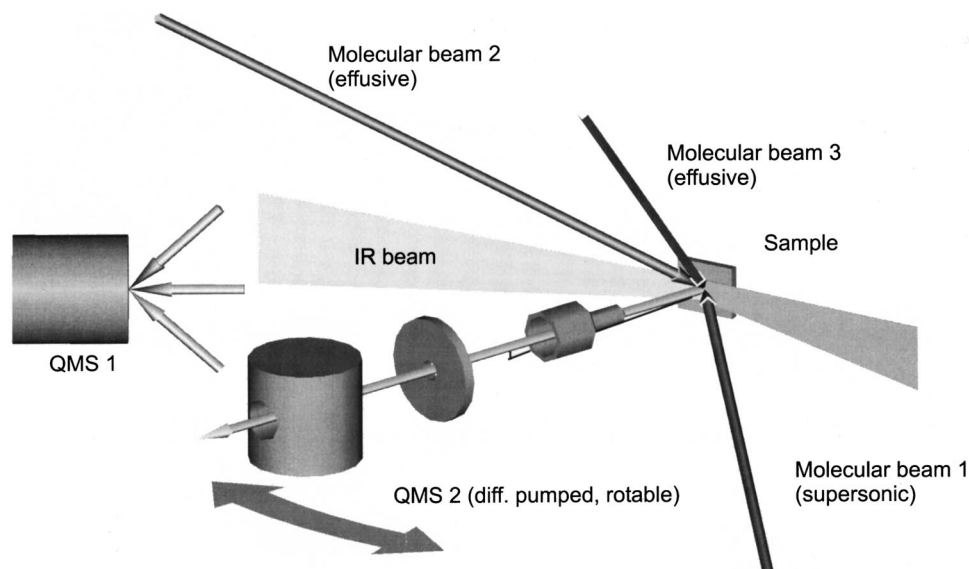

FIG. 1. Schematic representation of the molecular beam/IR spectroscopy experiment.

been prepared based on both, oxide single crystal surfaces (see Ref. 4 and references therein) and thin ordered oxide films.[15–19] Here, we will employ a Pd/Al_2O_3 model system based on a thin well-ordered alumina film prepared on NiAl(110). The structure and defect structure of the oxide film[20,21] as well as the growth, geometric structure, and electronic structure and the adsorption of Pd particles and other metals supported on this film have been extensively addressed in a series of previous studies.[15–17,19,22–24]

Once the structural properties of the supported model catalyst are well characterized, the next step is to establish a correlation between the structure and the microscopic kinetics. Here, molecular beam techniques represent the method of choice,[25–28] providing a maximum of control over the reactant flux and its interaction with the sample. Ertl and Engel[29,30] have early applied beam methods to study the kinetics of the CO adsorption and oxidation and on Pd(111). In this study, they were able to demonstrate that the reaction follows a Langmuir–Hinshelwood (LH) mechanism and they succeeded to determine the LH activation barriers in various coverage regions. A variety of similar studies on other single crystal surfaces have been published since (see, e.g., Refs. 31–33). The previous work on supported model systems has been reviewed recently, and will not be discussed here in detail.[4,22] It has to be pointed out, however, that, in spite of the successful experiments on single crystals, beam studies on the CO oxidation on supported catalysts are extremely rare. This is mainly due to the experimental problems mentioned before. As a consequence it remains unclear, to what extent size effects might be present on the system.[4] Among the few examples for beam studies on supported model catalysts, Stará *et al.* have studied the transient CO_2 production on Pd/Al_2O_3 as a function of particle size and substrate structure,[34,35] and found indications for significant size effects. No indications for a similar effect could be found in a recent study using the same model system as employed in this work.[36] Becker and Henry have investigated, by molecular beam methods, the CO oxidation reaction on Pd/MgO (100) model catalysts.[37,38] Variations in the steady state pro-

duction of CO_2 with particle size were observed. However, these differences in activity were mainly due to the effect of the capture, by the Pd particles, of the CO physisorbed on the support (reverse-spillover) which is equivalent to an increase of the effective pressure on the particles when their size decreases (see Sec. III H).[38] In addition, the transient behavior upon switching off the CO beam was considered in this work. A characteristic peak was found, the intensity of which increased with decreasing cluster size (for the same experimental conditions). The origin of this peak was attributed to low coordinated (edge and defect) sites, present on the supported particles. As has been proposed previously,[3] those sites may bind CO more strongly and thus they may give rise to a pronounced transient CO_2 production peak due to the increased residence time for CO at these sites.

In this study, we apply an experimental approach combining molecular beam techniques and TR-IRAS. We present a detailed study of the CO oxidation on well-shaped alumina supported Pd crystallites under steady-state and transient conditions. It is shown that the transient CO_2 peak, which is also found for the present model system, is not related to specific adsorption sites. Instead we discuss two points: First, we will show that the transient kinetics of the CO oxidation reaction—including the behavior of the CO_2 peak under discussion—can be qualitatively simulated from a simple ''mean-field'' kinetic model based on the data available on Pd(111). Secondly, we will argue, how the inherent heterogeneity of a supported catalyst may additionally enhance the observed effect.

II. EXPERIMENT

All experiments were performed in a new UHV molecular beam/surface spectroscopy apparatus at the Fritz-Haber-Institute (Berlin), which has been described in the literature, recently.[39] Schematically, the setup is displayed in Fig. 1.

The system has been specifically designed for kinetic studies on complex model systems. It offers the experimental possibility of up to three beams being crossed on the sample

TABLE I. Preparation conditions and structural parameters for the Pd particles on Al_2O_3/NiAl(110).

Deposition parameters		
Pd coverage (atoms·cm^{-2})	2.7×10^{15}	
Deposition temperature (K)	300	
Deposition rate (atoms·cm^{-2}·s^{-1})	9×10^{12}	
Structural parameters		
Island density (cm^{-2})	$1.0(\pm 0.2) \times 10^{12}$	(Refs. 22, 36)
Number of Pd atoms/island	~2700	(Refs. 22, 36)
Fraction of support covered by Pd	$0.20(\pm 0.02)$	(Refs. 22, 36)
Fraction of surface Pd atoms	$0.20(\pm 0.03)$	(Refs. 22, 36)
Average island size	5.5 ± 0.7 nm	(Refs. 22, 36)
Epitaxial orientation	(111)	(Refs. 16, 22, 24)
Island structure	crystalline, predominantly (111) facets, small fraction of (100) facets	(Refs. 22, 24)

surface. The CO and O_2 beams, which were mainly used in the work presented here, are generated by two effusive sources based on multichannel arrays. This design allows an easy variation of the beam intensities over several orders of magnitude, without any change in the beam properties. Beam modulation is provided by a computer-controlled shutter located inside the second pumping stage of the beam sources. To avoid artifacts due to only partial overlap, the beam diameter was chosen such that it exceeds the sample surface. The mean beam intensity variation over the sample surface was determined to be 6%. The average variation in the CO/O_2 beam intensity ratio over the sample surface was estimated to be less than 2% (from beam profile measurements). Both sources were operated at room temperature. High purity oxygen (AGA, >99.999%) and CO (AGA, >99.996%) were used, the latter of which was further purified using a $l-N_2$ cold trap;. The beam intensities and profiles were measured with a beam monitor as described elsewhere.[39] In order to avoid artifacts due to an effusive gas load upon closed beam at extreme CO/O_2 flux ratio, the CO_2 transients were recorded by opening/closing the inlet valves of the beam sources (pressure rising/dropping time, 500/2000 ms). The transient CO_2 peaks observed were in all cases significantly slower than the CO pressure change. At moderate flux ratio transients were recorded by modulating the beam source via the internal shutter (opening/closing time, 50 ms) to verify that there was no significant influence of the modulation procedure on the transient behavior. The third source generates a beam from a supersonic expansion and has not been used in the present study.

Angular-integrated gas phase measurements were performed with a quadrupole mass spectrometer (ABB Extrel) which is not in line-of-sight of the sample. Additionally, the systems allows time- and angular-resolved measurements via a differentially pumped rotatable quadrupole mass spectrometer. The gas phase detection can be combined with time-resolved *in situ* FT-IR reflection absorption spectroscopy (TR-IRAS) employing a vacuum FT-IR spectrometer (Bruker IFS 66 v). For the time resolved spectra with a temporal resolution of 1 s several transients were accumulated to improve the signal to noise ratio. For this purpose the beam shutter was synchronized with the recording of the IR spectra. Additionally, a MIR polarizer was used to select only the

p-component of the IR light and thus further improve the S/N ration. For a detailed description of the experimental details we again refer to the literature.[39] All spectra were recorded at a spectral resolution of 8 cm^{-1}. The total acquisition time for the *in situ* IR spectra was typically 50 s/spectrum and for the TR-IR spectra 5 s/spectrum.

Briefly, the sample was prepared by sputtering and annealing of a NiAl(110) single crystal, followed by an oxidation and annealing procedure, the details of which are given elsewhere.[20,21] The cleanliness and quality of the oxide film was checked via LEED and AES. Before the actual experiment, the active metal component (Pd, >99.9%) was deposited under well controlled conditions by evaporation from a rod (1 mm diam) using a commercial evaporator (Focus, EFM 3) based on electron bombardment. During deposition, the crystal was biased with a retarding voltage in order to prevent ions from being accelerated towards the sample (point defect creation). The evaporator flux was calibrated by a quartz microbalance prior to use. Details concerning typical deposition rates and conditions are given in Table I. After preparation the Pd particles were stabilized by oxygen and CO exposure as discussed previously.[36]

III. RESULTS AND DISCUSSION

A. Characterization of the structural and adsorption properties of the supported Pd model catalyst

The growth and structure of Pd deposits as well as other metals on Al_2O_3/NiAl(110) has previously been studied over a wide range of conditions and the results have been extensively reviewed, recently.[16,17,22–24] In this work, we will focus on one particular set of preparation conditions (substrate temperature, 300 K; Pd coverage, 2.7 $\times 10^{15}$ atoms cm^{-2}), for which detailed information on both the particle size and density and on the particle structure is available. In the following, we will briefly review the main features of this system. In Figs. 2(a) and 2(b) STM images (CCT, Constant Current Topography, from Ref. 36) are shown. The Pd particles form three-dimensional islands; their density typically amounts to 1×10^{12} islands cm^{-2}. From this number it can be estimated that the average Pd particle will contain about 2700 atoms, corresponding to an average particle size of 5.5 ± 0.7 nm. Please note that in the
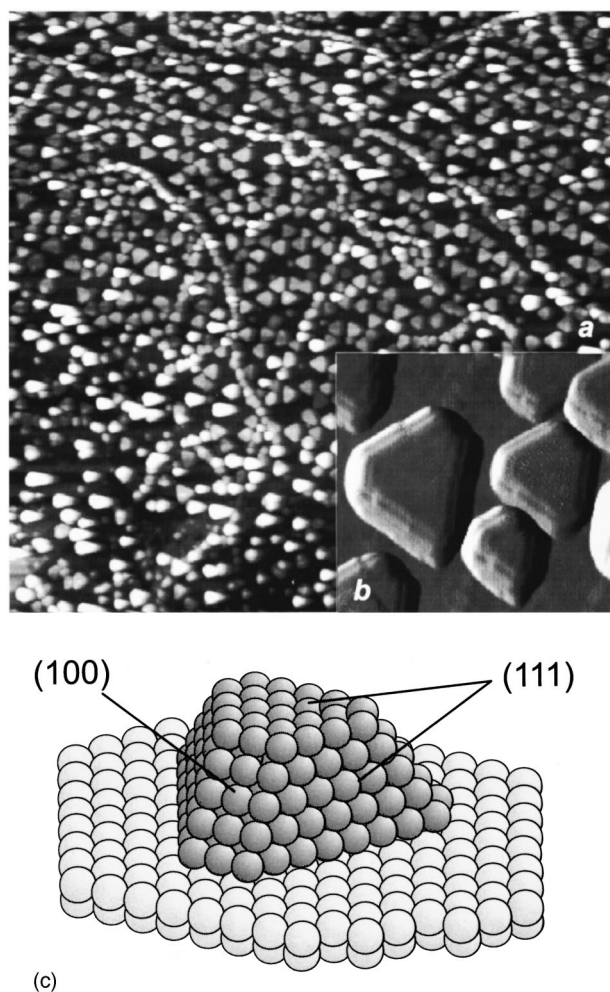
FIG. 2. (a) STM image (CCT, Constant Current Topography, 3000 Å ×3000 Å) of the Pd particles grown at 300 K on Al$_2$O$_3$/NiAl(110), from Ref. 36; (b) differentiated close-up STM image of the Pd particles (CCT, Constant Current Topography, 3000 Å×3000 Å), from Ref. 36; (c) schematic representation of a supported Pd particle.

STM image the islands appear larger than the above value due to an instrumental convolution with the tip shape. As a consequence of preferential nucleation the island appear not to be completely homogeneously distributed over the support but will decorate oxide point and line defects (e.g., domain boundaries, see Ref. 21). In the close-up shown in Fig. 2(b), it becomes evident that most of the Pd particles exhibit the well-defined morphology of a nanocrystallite. As indicated in the schematical representation [Fig. 2(c)], the particles grow in (111)-orientation, preferentially exposing (111)-facets and only a small fraction of (100)-facets. The regular structure of the Pd crystallites has been demonstrated in a recent STM study showing atomic resolution both on the top and side facets of the particles.[24] This and other structural information, which will be used in the following discussion, is summarized in Table I.

Before the kinetic experiments the particles were stabilized by extended oxygen exposure (typically ∼100 L, 1 L =1×10^{-6} Torr s), followed by several CO oxidation cycles of the type shown in this work. This stabilization procedure has been shown to be necessary to obtain a stable oxidation

kinetics.[36] As observed by STM,[36] neither the particle density nor the particle shape are significantly affected by the procedure. The chemical processes related to the stabilization procedure will be discussed elsewhere.[40]

Two types of experiments were performed to ensure that the model surface principally resembles the behavior of a typical Pd surface: (1) We have probed the CO adsorption/desorption kinetics employing modulated molecular beam techniques. In a temperature region from 430 to 530 K, we have determined an activation energy for desorption of 136 ±9 kJ mol^{-1} and a pre-exponential factor of 10$^{14.9±0.9}$ s^{-1} from the temperature dependence of the CO residence time in the low CO coverage region. Details of the experiment will be given elsewhere.[41] This value is in excellent agreement with experiments on a Pd(111) single crystal [desorption energy, 134±8 kJ mol^{-1}, pre-exponential factor, 10$^{14.4±0.8}$ s^{-1} (Ref. 30)]. (2) The activation barrier for the Langmuir–Hinshelwood reaction step has been determined in a series of beam experiments at high oxygen (and CO) coverages.[36] The apparent activation barriers of 62 ±8 kJ mol^{-1} (and 59±8 kJ mol^{-1}) are as well in good agreement with Pd(111) single crystal data [59±8 kJ mol^{-1} (Ref. 29)] under similar conditions. Thus we conclude that the general adsorption and reaction behavior of the supported model catalysts under consideration appears rather similar to that of a Pd(111) single crystal surface In the following sections we will investigate the steady state and in particular the transient CO$_2$ production in more detail. Thus we will attempt to elucidate, whether the reaction behavior of the system may still differ from the single crystal and how these differences might be addressed experimentally.

B. General types of transient behavior

Before we come to a systematic discussion of the transient and steady-state behavior of the CO oxidation, we will give a short description on how most of the experiments in this study were performed and how the different types of transients can be qualitatively understood.

The general types of CO$_2$ transients are shown in Fig. 3. The corresponding experiments were performed in the following manner: After preparation and stabilization of the model system, the surface is continuously exposed to an O$_2$ beam with a beam flux F_{O_2}, generated by one of the effusive beam sources (see Fig. 1). The integral CO$_2$ production rate is recorded simultaneously. At a time $t_{CO,on}$ (see Fig. 3) a CO beam with a beam flux F_{CO}, generated by the second effusive source (see Fig. 1), is switched on. As flux parameters we define (1) x_{CO}, the CO fraction with respect to the total flux, as

$$x_{CO} = \frac{F_{CO}}{F_{CO} + F_{O_2}} \qquad (1)$$

and (2) p_{total}, the total effective pressure of CO and O$_2$ at the sample position,

$$p_{total} = p_{CO} + p_{O_2} \quad \text{with} \quad p_i = F_i (2\pi m_i kT)^{0.5}, \qquad (2)$$
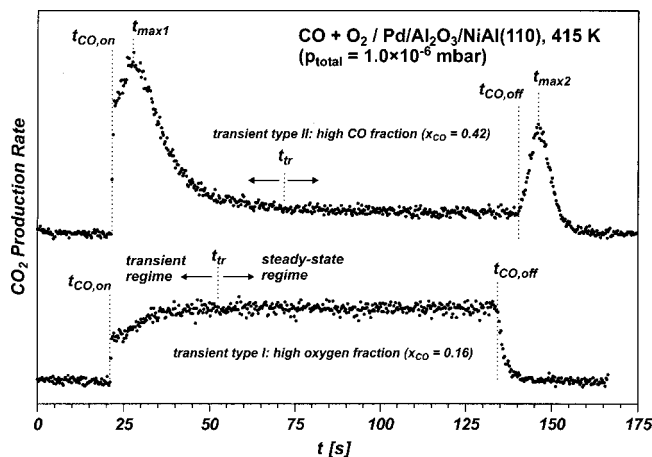
FIG. 3. Transient behavior of the CO_2 production rate (continuous O_2 beam and a modulated CO beam) under CO-rich conditions (upper trace, transient type II) and O_2-rich conditions (lower trace, transient type I) ($T_{Sample} = 415$ K, $p_{total} = 1.0 \times 10^{-6}$ mbar).

where F_i is the partial flux of component i at the sample position, m_i represents its molecular mass, and T_i is the temperature describing the velocity distribution (please note that $T_i = 300$ K as there is no cooling of any degree of freedom in the effusive sources). Typically, in a series of experiments, the CO flux fraction was varied, whereas the other parameters such as the total effective pressure, the sample temperature etc. were kept constant.

In general two different types or transients can be observed as a function of the CO flux fraction, which, in the following, we will denote as type 1 and type 2 (see Fig. 3), respectively. The initial transient behavior has recently been discussed by Piccolo et al.[42,43]

Type 1: If the experiment is performed at low CO and high O_2 flux, a simple type of transient behavior is observed as displayed in the lower trace in Fig. 3 ($x_{CO} = 0.16$). We start from a situation, in which the system has reached its oxygen saturation coverage under the given flux and temperature conditions. Upon switching on the CO beam ($t_{CO,on}$), we find an instantaneous increase (on the time scale of the experiment) in the CO_2 production. As pointed out by Piccolo et al.[43] this is due to the rapid formation of a steady-state precursor coverage. From this precursor, the CO molecule may either desorb or chemisorb and subsequently react to CO_2. In the course of the reaction oxygen vacancies are generated, which lead to an increased adsorption probability for the CO precursor and thus an increase in the reaction rate. After this transient period (t_{tr}), the system finally reaches the steady-state reaction conditions. Please note that the steady-state is characterized by a high oxygen coverage and low CO coverage. After switching off the CO beam ($t_{CO,off}$), the adsorbed CO is consumed and the CO_2 production rate decreases continuously.

Type 2: If an equivalent experiment is performed at sufficiently high CO fraction (Fig. 3, upper trace, $x_{CO} = 0.42$), a different behavior is found. Again, starting from an oxygen saturated surface, we observe an instantaneous increase in the CO_2 production rate upon switching on the CO beam. Subsequently, the reaction rate increases slowly until it

reaches a first maximum (Fig. 3, $t_{max\,1}$). As for transient type 1, the increasing reaction rate can be explained by an increasing chemisorption probability of the CO precursor, due to the decreasing oxygen coverage.[43] Once a certain CO coverage is reached, however, the CO oxidation rate decreases again. This is a consequence of the strongly inhibiting effect of CO on the O_2 adsorption (for a general discussion see, e.g., Ref. 44, and references therein). Finally, a steady-state is reached, which is characterized by a high CO coverage and a low reaction rate (due to the inhibiting effect of CO). Once the CO beam is terminated ($t_{CO,off}$), the process is reversed: the adsorbed CO is consumed in the course of the reaction, leaving free adsorption sites for O_2 adsorption. Thus the O_2 adsorption is accelerated and so is the reaction rate, which reaches a maximum ($t_{max\,2}$), before it finally decreases due to depletion of the CO reservoir.

C. Catalyst stability under reaction conditions

In a second step, we will briefly consider the catalyst stability under the reaction conditions applied in this study. There are two main processes which may have an influence on the catalytic activity: (1) Prolonged exposure to the reactant gases in combination with elevated reaction temperatures may lead to structural rearrangements or changes in the particle dispersion. For example, in a recent study it has been shown that Pd particles may undergo drastic shape variations under the influence of oxygen.[45] (2) CO dissociation may lead to a build-up of surface carbon, which may result in a deactivation of the catalyst. The formation of surface carbon has previously been observed for the CO oxidation reaction on small Pd particles[46] and there have been indications for carbon formation on Pd single crystal surfaces at higher CO pressure.[47]

Concerning a possible restructuring of the particles we refer to a previous study focusing on the interaction of oxygen with the same Pd model catalyst and its influence on the kinetics of the CO oxidation.[36] It was shown that under the reaction conditions applied here, neither the Pd particle shape nor the particle dispersion are significantly affected by the oxygen pretreatment or by subsequent oxidation cycles. With respect to the possibility of surface carbon formation, we consider the experiment displayed in Fig. 4. Four different transients at high CO flux fraction (transient type II) are shown for comparison. The transients were recorded under identical conditions directly after an initial extended oxygen exposure (oxidation cycle 1), and after 1 to 22 subsequent transient experiments (see Fig. 4). It is found that neither the steady-state CO_2 production rate nor the shape or the intensity of the second CO_2 peak (after termination of the CO beam) changes as a function of reaction time. The only observable change is related to the initial CO_2 production peak, which is slightly smaller during the first oxidation cycles.

As mentioned before, in a recent work employing STM,[36] we could exclude major structural rearrangements such as a spreading of the Pd under the influence of the oxygen as an origin of the increased adsorption capacity after several adsorption/reaction cycles. In the same study, however, a strongly reduced CO_2 peak was found before ex-

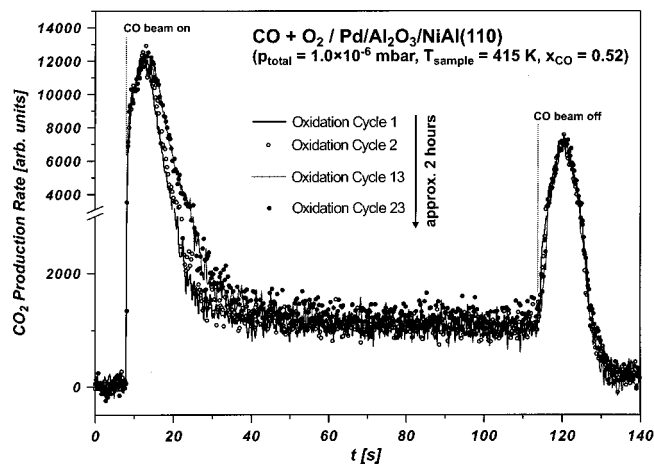FIG. 4. Comparison of the transient behavior of the CO_2 production rate under identical conditions as a function of reaction time ($T_{Sample}=415$ K, $p_{total}=1.0\times10^{-6}$ mbar).

tended oxygen exposure. This observation suggests that also in the initial cycles shown in Fig. 4 the stabilization process (see Sec. III A) is not fully completed, leading to a loss of oxygen on the Pd particles during the experiment. After the initial cycles a stable oxidation kinetics evolves, showing global desorption and reaction rates consistent with previous experiments on Pd(111) surfaces (see Sec. III A).

Another indication that there is no significant carbon formation, is derived from the *in situ* IR spectra, which will be discussed in Sec. III E. For CO dissociation on Pd(111) Hammoudeh[47] has shown that surface carbon formation results in a strongly enhanced occupation of on-top sites. No indications for such changes have been found in the present experiments.

Thus we may conclude that under the reaction conditions and time-scales applied here, there is no substantial deactivation mechanism present, which may significantly affect the results presented in the following sections.

D. Systematic studies of the transient behavior and steady-state CO_2 production

In order to obtain a general overview over the reaction behavior we have performed a series of transient beam experiments at different reaction temperatures. A typical series of experiments at a sample temperature of 440 K is displayed in Fig. 5. The sample was exposed to a continuous oxygen beam. Its intensity was chosen such that the total effective pressure after switching on the CO beam was $p_{total}=1.0\times10^{-6}$ mbar. The CO flux fraction x_{CO} was varied between 0.05 and 0.95 and for each x_{CO} a transient was recorded.

In general, we find the two types of transient behavior, discussed in Sec. III B. For $x_{CO}\leq0.37$ the transients are of type 1 (oxygen-rich steady state, see Fig. 3), whereas for $x_{CO}\geq0.47$ we find a CO rich steady-state, connected with the characteristic CO_2 production rate maxima (transient type 2). The transition region between the two regimes will be discussed separately in Sec. III F.

We start considering some basic features of the experiment. With respect to the characteristics of the first transient CO_2 peak, it is found that the time constant at which the steady-state is reached after switching on the CO beam diverges close to the transition region. This is easy to understand as the CO coverage is build up by the excess of adsorbed CO (not consumed during the reaction), which vanishes at the transition between the two regimes. The integral below the transient peak, however, remains nearly constant for $x_{CO}\geq0.52$. This is explained by the fact that the peak integral roughly corresponds to the oxygen precoverage, which is constant and will be fully consumed during the reaction. Contrary to the first transient peak, the width of the second transient peak (upon switching off the CO beam) increases with increasing x_{CO} since the O_2 flux and therefore the reaction rate decreases. The integral over the second transient peak as a function of x_{CO} will be considered in detail in Sec. III F. It corresponds to the fraction of CO adsorbed in the steady-state that upon termination of the CO beam will not desorb but react to CO_2. In general, it will show a step-like behavior similar to the first transient peak. In contrast to the adsorbed oxygen, the CO, however, may desorb on the time-scale of the reaction at high reaction temperatures and low O_2 flux, which may lead to a decreasing peak integral at high x_{CO}.

From the transients in Fig. 5 we can derive a plot of the steady state reaction rate as a function of the CO flux fraction x_{CO} as displayed in Fig. 6. Qualitatively, it can be understood as follows: At low x_{CO} (on the oxygen-rich side), the CO_2 production is proportional to the CO partial pressure. It reflects the sticking coefficient of CO under the particular steady-state conditions, i.e., under high oxygen and low CO coverage. At a certain critical x_{CO}, the system switches from
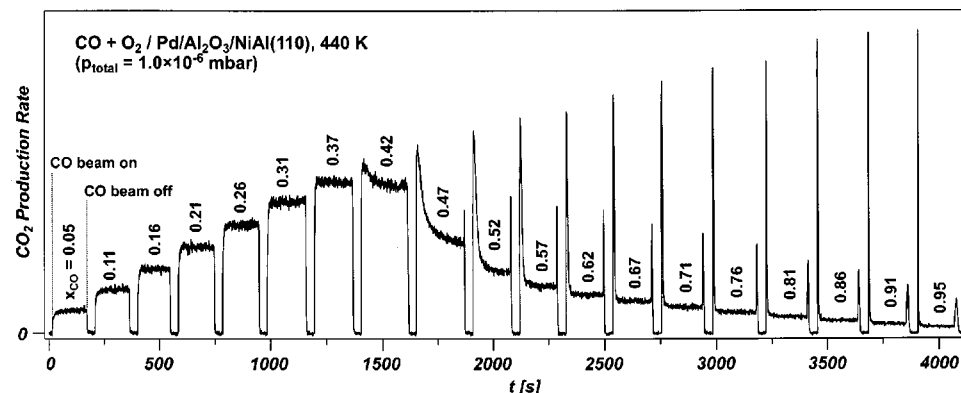

FIG. 5. Transient behavior of the CO_2 production rate as a function of the CO fraction in the impinging gas flux x_{CO} ($T_{Sample}=440$ K, $p_{total}=1.0\times10^{-6}$ mbar).
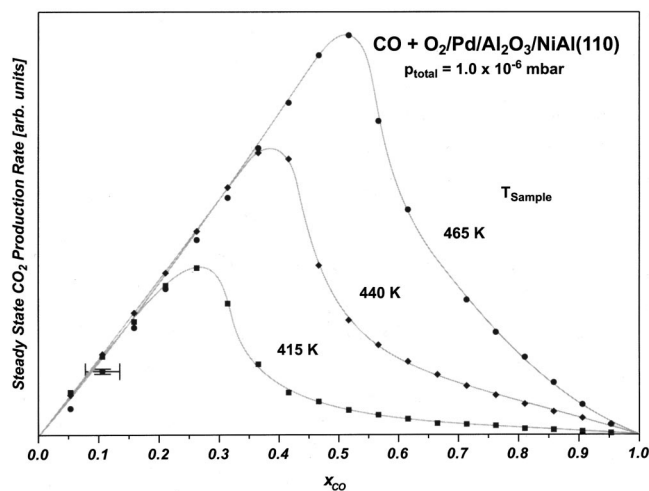
FIG. 6. Steady-state CO_2 production rate as a function of the CO fraction in the impinging gas flux x_{CO} ($p_{total} = 1.0 \times 10^6$ mbar).

an oxygen-rich to a CO-rich steady-state. This transition appears to occur continuously over a significant range of flux ratios, which will be discussed in detail in Secs. III F–III H. The transition is connected to a sudden decrease in the reaction rate as a consequence of the inhibiting effect of CO on the dissociative adsorption of O_2 (see, e.g., Ref. 44).

Comparing the three different reaction temperatures displayed, we find a behavior which is easily explained qualitatively: In the low CO coverage region, the reaction rate is almost independent of reaction temperature. This indicates similar steady-states under these conditions which are close to oxygen saturation. Generally, the CO sticking coefficient, which governs the reaction rate, is expected to decrease slightly with increasing temperature due to the decreasing lifetime of the CO precursor state both on the alumina substrate and on the Pd particles. This effect, however, is too weak to be identified clearly from the present data. Note that although the CO steady-state coverage is small, it will depend on the reaction temperature, i.e., the steady-state CO coverage will increase with decreasing surface temperature. Therefore, at low temperature the transition point, at which due to inhibition of oxygen adsorption the system switches to the CO-rich state, is reached at lower x_{CO}. In the high CO coverage region the rate is limited by the oxygen adsorption step. The reaction rates do not coincide due to the increased CO steady-state coverage at lower temperatures (slower desorption and reaction rates) which give rise to an increased inhibition of the O_2 adsorption.

Similar data have been derived for the CO oxidation on a number of catalytically active transition metal surfaces. As the most relevant reference case we briefly consider the work of Hammoudeh,[47] who has studied the CO and O_2 adsorption and CO oxidation on Pd(111) applying in situ IR and work-function measurements. It was shown that the reaction rate on Pd(111) exhibits a rather complex behavior, showing two maxima/hysteresis regions as a function of the reactant fluxes. Both strongly depend on certain internal parameters such as the pretreatment of the sample. Hammoudeh connected the first maximum to the inhibition effect explained

above and tentatively assigned the second maximum to reactivity variations related to changes in the dispersion of adsorbed CO islands. In the case of small metal particles, the formation of large adsorbate islands may be prevented by the limited size of the crystallite facets. This, as a general difference between single crystal and supported particle systems, may—among other effects—give rise to a suppression of a second reactivity maximum and thus to a simpler overall behavior of the reaction system.

Moreover, it was observed in the same study[47] that the kinetics is not stable under certain reaction conditions, but gradually changes during the reaction itself. This behavior was related to the slow formation of subsurface and bulk oxygen and the situation was found to be stabilized after prolonged oxygen exposure. In accordance with this interpretation, we find that the oxygen-pretreated particles used in this study, show a stable oxidation kinetics, even after repeated oxidation-reduction cycles.

In future work, the data of the type presented here, may provide a basis for more extensive microkinetic simulations of the steady state and transient reaction behavior. It has to be pointed out that such simulations—in connection with steady-state reaction rate measurements for different types of structurally well-characterized supported model catalysts—may be an excellent tool to identify kinetic effects characteristic for supported nanoparticles.[5] In a recent series of papers Zhdanov and Kasemo have discussed this issue[5–7] in connection with two types of effects, namely, the influence of communication between different facets on the nanocrystallites and the role of support mediated adsorption.

E. In situ IR absorption spectroscopy under steady-state conditions

In order to obtain further insight into the occupation of CO adsorption sites under steady-state conditions, we have acquired IR reflection absorption spectra under reaction conditions. The spectra were taken after the steady-state was reached in transient experiments of the type shown in Fig. 5. For the example displayed in Fig. 7 the surface temperature was 415 K.

Based on a comparison with IR spectra of CO on different Pd single crystal surfaces,[48–55] we may assign the observed features. Tüshaus,[52] for example, has studied CO on clean and roughened Pd(111) surfaces. Hammoudeh[47] has investigated the coadsorption of oxygen and CO using IR spectroscopy. The spectral features observed for CO adsorbed on Pd particles supported on Al_2O_3/NiAl(110) were previously investigated by Wolter et al.[23] over a large range of surface coverages and at different sample temperatures. At room temperature (and above) three types of adsorbed CO can be identified. At low coverage CO adsorbed in hollow sites is the dominating species ($\sim$1830 cm^{-1}), mainly from threefold hollow sites on the (111)-facets, since there will be only a small fraction of CO adsorbed on the minority of (100) sites and the signal will be additionally damped due to the inclination angle with respect to the sample. With increasing coverage an increasing occupation of bridge sites ($\sim$1900–1950 cm^{-1}) is observed. In contrast to low sample temperatures, however, thermal line-broadening at room
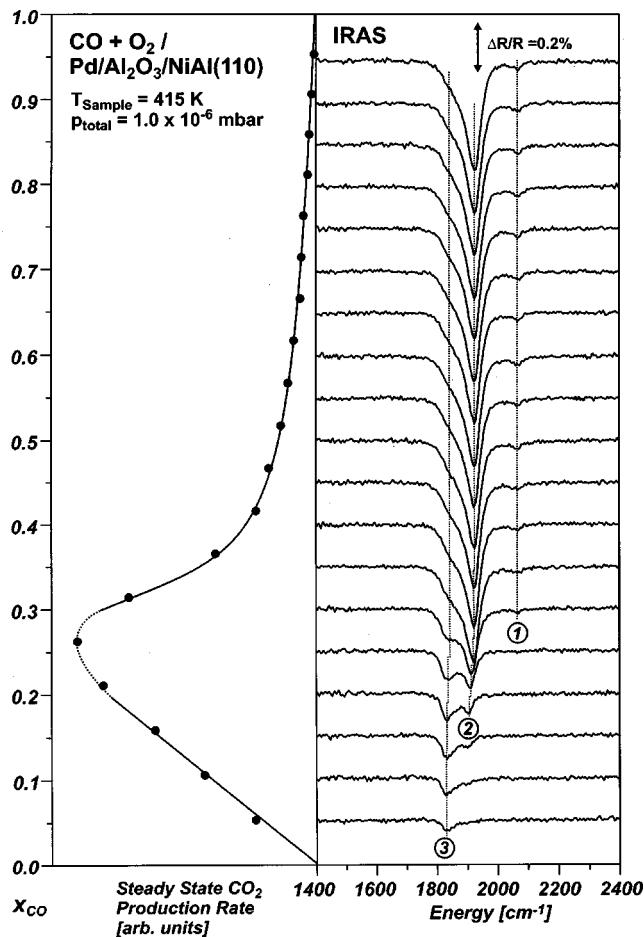
FIG. 7. *In situ* IR reflection absorption spectra under steady-state reaction conditions as a function of the CO fraction in the impinging gas flux x_{CO} (T_{Sample}=415 K, p_{total}=1.0×10^{-6} mbar).
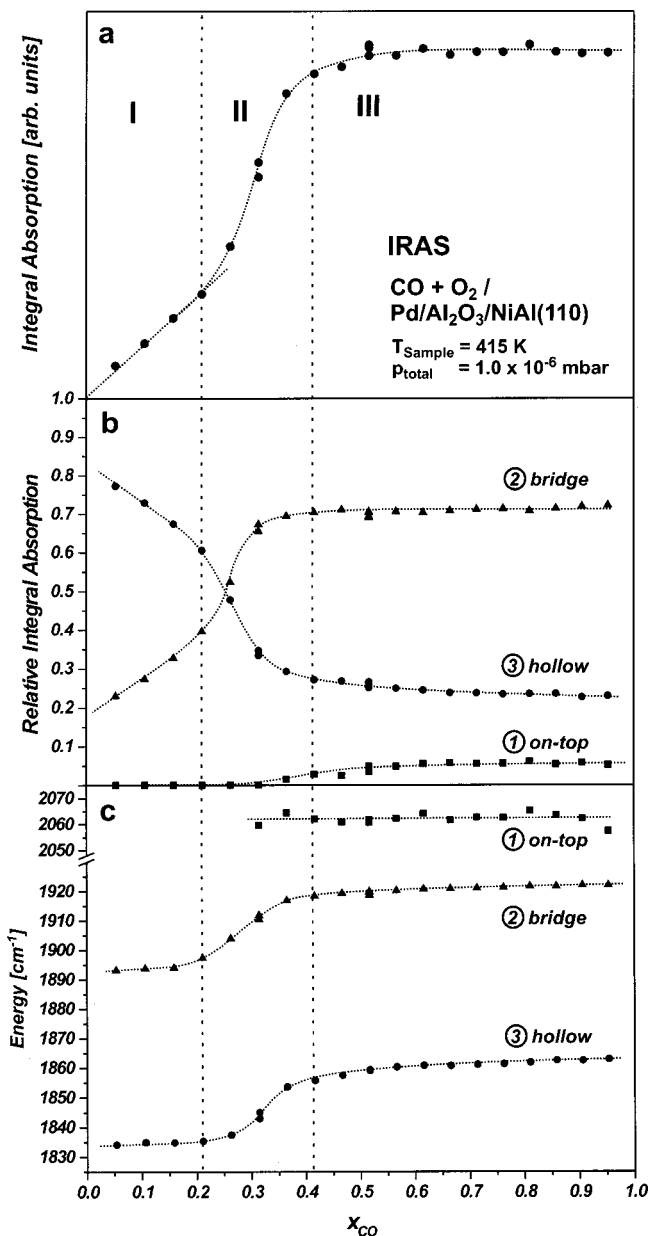

FIG. 8. (a) Integral absorption for the IRA spectra presented in Fig. 7; (b) relative absorption in the regions characteristic for CO adsorbed in (1) on-top, (2) bridge-bonded, and (3) hollow sites; (c) vibrational frequencies of the CO species marked in (b). Additionally, the oxygen-rich region (I), the CO-rich region (III), and transition regime (II) are indicated.

temperature and higher prevents a differentiation between CO bonded to regular and defect sites.[23] With the surface coverage increasing further, a weak absorption signal in the energy region typical for terminally bonded CO appears ($\sim$2060 cm^{-1}).

Qualitatively, the CO spectra under steady state reaction conditions (Fig. 7) appear very similar to the observations for adsorption of pure CO described above. CO bonded in hollow sites (Fig. 7, No. 3), in bridge sites (Fig. 7, No. 2) and on-top CO (Fig. 7, No. 1) can be distinguished. The quantitative development of the IR spectra as a function of x_{CO} is displayed in Fig. 8. The integral CO absorption signal [Fig. 8(a), regime I] initially (below x_{CO}=0.2) increases almost linearly with increasing CO flux fraction. This observation is in line with a LH rate constant being largely independent of CO coverage in the low CO flux limit (note that the IR absorption will be almost linear with the coverage in the low coverage limit, whereas at high coverages strong deviations may occur, see, e.g., Refs. 48, 56–58). In the transition region (Fig. 8, regime II), where the systems switches to the CO-rich reaction regime, the CO absorption signal increases rapidly, indicating also a sudden increase in CO coverage. From this point on (Fig. 8, regime III, x_{CO}>0.4), hardly any further changes can be detected in the CO absorption spectrum.

Figure 8(b) shows the relative fraction of the three principal CO species as derived from a fit of the spectra displayed in Fig. 7. At low x_{CO}, CO in hollow sites represents the majority species. The fraction of bridge CO increases slowly with increasing CO fraction, before in the transition regime a sudden increase in the population of bridge sites is observed, whereas the signal from the CO in hollow sites remains almost constant. Simultaneously, a small fraction of CO populates on-top sites. In comparison to single crystals, this on top signal under steady-state conditions appears at lower energies (2062 cm^{-1}) and is present at lower sample temperatures (Ref. 47, see also Refs. 51 and 53). This effect may be related to adsorption at typical defect sites on the supported particles such as steps or edges.

In Fig. 8(c) we investigate the influence of the CO flux fraction x_{CO} on the CO stretching frequency. The data was also derived from fits of the spectra displayed in Fig. 7. As has been discussed early (see, e.g., Ref. 59, and references therein), the CO stretching frequency may serve as a measure of the local CO density. The shifts are mainly due to two effects, namely changes in the CO–Pd bonding induced by neighboring CO molecules (chemical effects) or by coupling of the dynamic dipoles.[59] Quantitatively, the contributions for Pd(111) have been estimated by Tüshaus.[52] It has to be pointed out that a quantitative relation of the CO stretching frequency to the local CO coverage is complicated by the influence of coadsorbed oxygen, which also perturbs the electronic structure of Pd and thus the Pd–CO bond. For example, Hammoudeh[47] has shown that preadsorbed oxygen on Pd(111) may result in a shift of the CO singleton frequency from 1803 cm^{-1} to 1822 cm^{-1}.

Although these effects preclude a straightforward quantitative analysis, we may, however, derive some indications on the CO distribution from the vibrational frequencies displayed in Fig. 8(c). Up to a x_{CO} of 0.2, the shift in the stretching frequency of CO bound to hollow sites is small (~ 1 cm^{-1}), indicating that there are only minor changes in the local environment of adsorbed CO molecules. Similarly, this observation holds for CO bound to bridge sites up to $x_{CO} \lesssim 0.2$. Thus, we may conclude that the formation of increasingly large CO islands under these conditions is unlikely and the CO can be anticipated to exist in a largely diluted form in an oxygen-rich surrounding. The local CO density changes suddenly and almost exclusively in the transition range between the oxygen-rich and the CO rich regime. This is indicated by a shift of approximately 28 cm^{-1} to higher frequency, both for the CO in bridge and hollow sites.

The transition between the two regimes, however, does not show a step-like behavior, but continuously extends over a finite range of x_{CO} values. This effect will be further discussed in the following sections.

F. Transient CO switching-off behavior

Among the different kinetic effects on supported catalysts, surface diffusion mediated coupling between different types of adsorption sites has recently attracted considerable attention.[5–7] The presence of different types of adsorption sites in close proximity is an intrinsic property of complex catalytic systems. Such types of adsorption sites may, e.g., be different facets on nanocrystallites, step, edge or other defect sites, interface sites located at the particle boundary or adsorption sites on the support material itself. Zhdanov and Kasemo[5] have extensively reviewed simulations of such coupling processes. They have shown that relatively moderate changes in the sticking coefficients or reaction/adsorption energetics may drastically change the reaction rate under certain conditions.

Still, the experimental verification of these effects is not straightforward and very few examples exist in the literature. Recently, Becker and Henry have observed a transient behavior in an experiment, similar to the transient experiments shown in this work, which was related to such an heterogeneity effect.[4,37,38] Upon switching-off the CO beam, they observed a sudden decrease of the CO_2 production rate, followed by a smaller CO_2 production peak.

Becker and Henry originally suggested an explanation,[4,37,38] followed by simulations,[60] which involves rapid desorption of CO from regular sites (resulting in the rapid decrease in CO_2 production). Based on previous studies,[3,61] CO adsorbed at low coordinated edge sites (the proportion of which is increasing with decreasing cluster size), is assumed to be bound more strongly. Thus these sites will remain fully saturated until the CO reservoir on the facets is largely depleted. Only after vacancies among these defect are generated, the reaction rate increases again. This effect is assumed to result in the smaller maximum in the CO_2 production rate.

Since the Pd crystallites in the present study are composed of similar facets (111) and (100), a similar effect is expected for the present model system, but with a weak second peak due to the rather large particle size. Therefore, we have investigated the transient behavior under a variety of flux and temperature conditions (Fig. 9). Indeed, we find that under certain flux conditions we observe a transient CO_2 peak, which appears very similar to the effect originally reported by Becker and Henry. After an initial sudden decrease in the reaction rate, the CO_2 production shows a peak, which strongly depends on the experimental conditions. The effect only starts to appear close to the transition between the oxygen-rich and the CO-rich reaction regime.

To further investigate the origin of the peak, we have systematically varied the CO flux fraction x_{CO} between both reaction regimes. The result for two reaction temperatures is displayed in Fig. 9. The inset shows the integral CO_2 production in the switching-off peak. As a function of x_{CO} the intensity varies continuously. At high CO ratio it develops into the typical transient peak observed at high CO coverage, which is a simple consequence of the inhibiting effect of CO on the O_2 adsorption. At low CO fraction it first decreases and finally vanishes completely.

In contrast to the previously suggested explanation, this continuous intensity variation indicates that the effect, at least for the present supported model catalyst is not related to a characteristic type of defect sites connected to the Pd particle size. Instead, the effect appears to involve all CO adsorption sites available on the particle.

The crucial point with respect to the previous explanation is related to the assumption that the sudden decrease in the reaction rate is related to the spontaneous desorption of CO upon termination of the CO beam. To verify, whether such an effect exists, we have performed a time-resolved *in situ* IRAS experiment [see Fig. 10(b)] simultaneously with the reactivity measurements [Fig. 10(a)]. Under conditions, where the sudden decrease and transient peak are observed we have recorded IR absorption spectra with a temporal resolution of 1 s. In order to improve the signal/noise ratio the full reaction sequence was automatically repeated. In Fig. 10, spectra which were obtained by accumulation of 5 transients are displayed. The IRA spectra (bridge and hollow absorption peaks) were integrated and the results are shown in the inset [Fig. 10(c)]. No indication for a sudden decrease
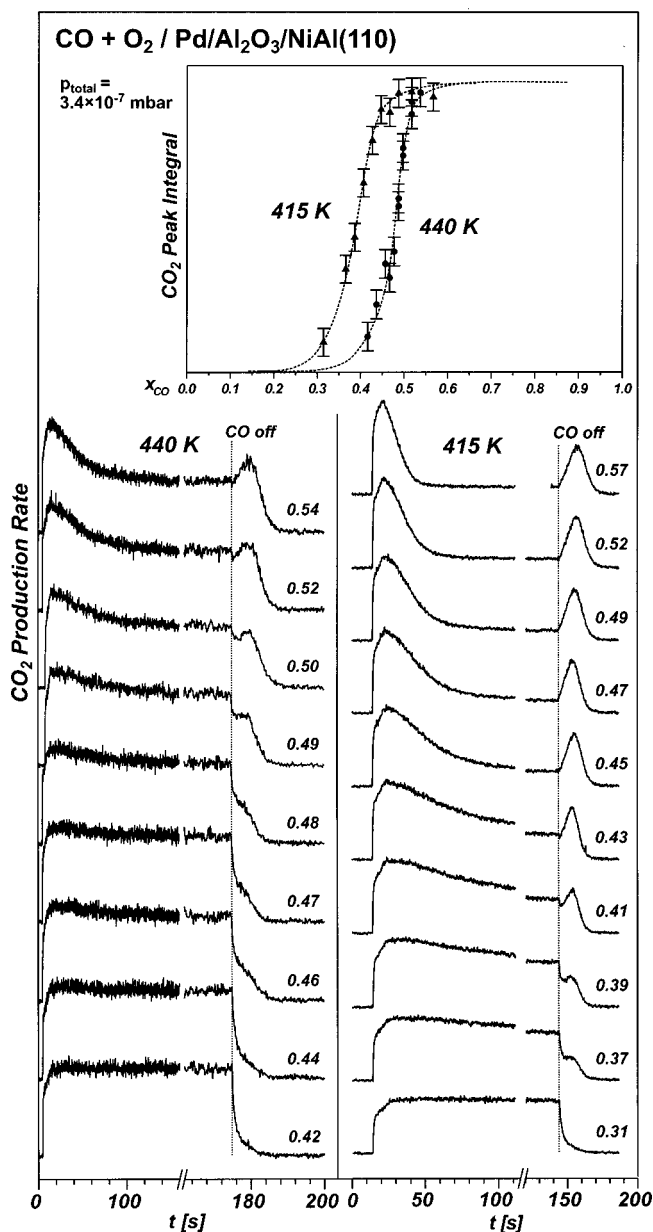
FIG. 9. Transient behavior of the CO_2 production rate as a function of the CO fraction in the impinging gas flux x_{CO} close to the transition between the two reaction regimes ($p_{total} = 3.4 \times 10^{-7}$ mbar). The inset shows the integral over the peak which appears upon termination of the CO beam.

temperature of 415 K (440 K) at low CO coverage. Indeed, this estimate indicates that no sudden desorption is expected on the time scale under discussion. In the following we will discuss, which alternative effects may have to be taken into consideration in order to account for the observed transient behavior.

The experiments discussed before, have shown that the CO_2 peak (1) starts to appear only in the transition between the two reaction regimes and (2) is not related to specific defect sites (at least for the model system studied here). Taking this into account we may consider the following alternative explanations, which may give rise or additionally contribute to the observed effect:

(1) *Local beam intensity variations:* Due to beam intensity variations in the CO and O_2 beam, the sample surface will locally be exposed to different effective pressures and flux ratios. From beam profile measurements, a standard deviation of the local pressure p_{eff} of typically $\pm 6\%$ can be estimated. The standard deviation of the flux ratio x_{CO} is typically $\pm 2\%$. The width of the transition region (see Fig. 9), however, is significantly broader (typically in the order of $\pm 10\%$ of the x_{CO} value at which the transition occurs). Thus, in a first approximation this contribution may be neglected.

(2) *CO poisoning induced peaks:* As discussed in Sec. III G, the transient behavior can be semiquantitatively simulated using a simple homogeneous ''mean-field'' model based on kinetic parameters from separate adsorption and reactivity studies on Pd(111) and the supported Pd particles. It is shown that the transient CO_2 production rate in the transition region may show a behavior similar to the one observed experimentally, as a consequence of the competition between the decreasing CO coverage and increasing O_2 sticking probability.

(3) *Effects induced by the heterogeneity of the system:* The effect, described in (2) may be additionally enhanced by the inherent heterogeneity of the supported model catalyst. On the model surface, every Pd particle represents a largely isolated reaction system. Yet, the individual adsorption and reaction rates may differ considerably. Thus, different steady states may coexist under given conditions, with the total reaction rate being a superposition of the individual states. The influence of this effect on the transients will be discussed in Sec. III H.

G. Simulations

It has been shown in the previous section that the peculiar transient behavior of the reaction rate was not related to the presence of specific highly-binding sites on the clusters. At this point it is tempting to simulate the steady state and transient experiments on the basis of a ''mean-field'' kinetic model of a homogeneous surface. Such modeling may provide some indications, which features may at least qualitatively be described by the simple kinetic model and where the complexity of the system will have to be explicitly considered in the model.

Let us consider a Pd(111) single-crystal surface. Adsorbates are supposed to be randomly distributed on this sur-

in the CO absorption signal is found. Instead the absorption peaks decreases continuously with a slope roughly resembling the reaction rate (note that due to the nonlinear coverage-absorption dependency there is no simple correspondence between the two quantities, see Sec. III E)

This result, in line with the previous intensity argument (Fig. 9), clearly demonstrates that the observed behavior cannot be a result of spontaneous CO desorption from regular sites and strong binding to defect sites. Instead, the effect appears to be related to the simple CO_2 production peak under conditions of high CO flux. This suggestion is consistent with an estimate of the CO surface residence times based on the desorption data given in Sec. III A ($E_{a,des} = 136 \pm 9$ kJ mol^{-1}, $A_{des} = 10^{14.9 \pm 0.9}$ s^{-1}). Using these values, we calculate a residence times of 200 s (20 s) for a surface
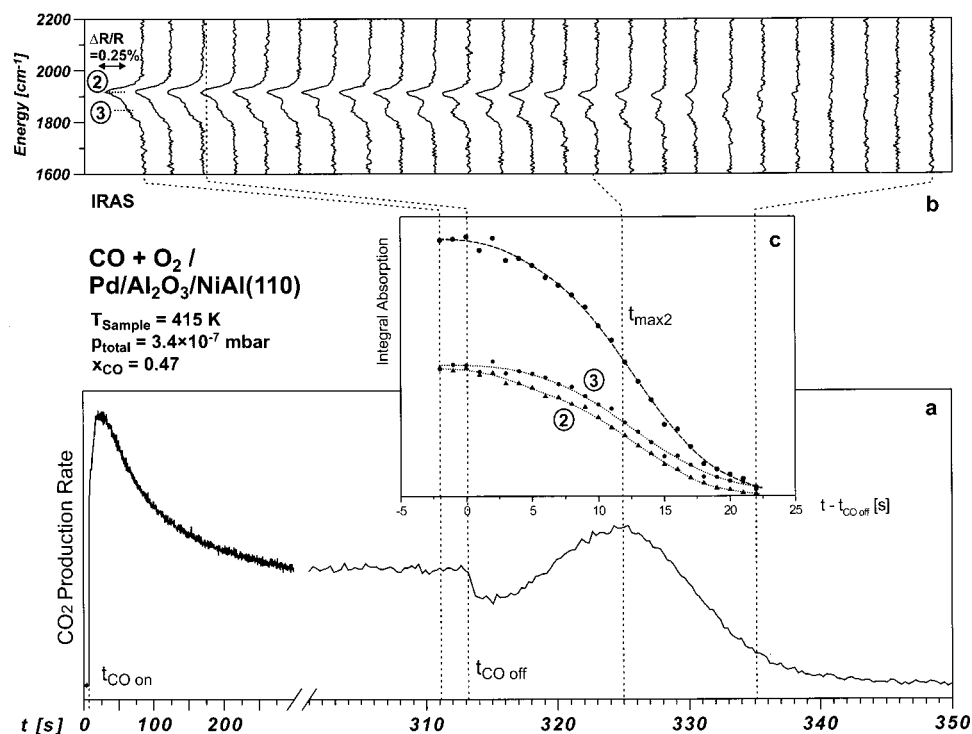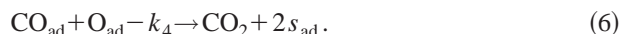
FIG. 10. Combined reactivity (a) and time-resolved IR reflection absorption experiment (b) during the transient region upon termination of the CO beam ($T_{\text{Sample}} = 415$ K, $p_{\text{total}} = 3.4 \times 10^{-7}$ mbar). (c) Integral absorption for the IRA spectra presented in (b) and partial absorption in the bridge (2) and hollow (3) regions.

face. The overall CO oxidation reaction can be expanded in its elementary steps:

$$CO + s_{ad} - k_1 \rightarrow CO_{ad}, \qquad (3)$$

$$CO_{ad} - k_2 \rightarrow CO + s_{ad}, \qquad (4)$$

$$O_2 + 2s_{ad} - k_3 \rightarrow 2O_{ad}, \qquad (5)$$

$$CO_{ad} + O_{ad} - k_4 \rightarrow CO_2 + 2s_{ad}. \qquad (6)$$

s_{ad} refers to a free adsorption site. k_i is the rate constant of step i.

The CO_2 desorption step ($CO_{2ad} \rightarrow CO_2$) being much faster than the other steps,[29] it is not necessary to expand step (4). Equations (3)–(6) can be converted to the following system of coupled differential equations, which describes the time evolution of the CO coverage θ_{CO} and of the oxygen coverage θ_O (see, e.g., Ref. 42),

$$\frac{d\theta_{CO}}{dt} = k_1 S_{CO} - k_2 \theta_{CO} - k_4 \theta_{CO} \theta_O$$

with

$$S_{CO} = S_{CO}^0 \left(1 - \frac{\theta_{CO}}{\theta_{CO}^{max}} - C_{T_s} \frac{\theta_O}{\theta_O^{max}} \right), \qquad (7)$$

$$\frac{d\theta_O}{dt} = 2k_3 S_{O_2} - k_4 \theta_{CO} \theta_O$$

with

$$S_{O_2} = \begin{cases} S_{O_2}^0 \left(1 - \frac{\theta_{CO}}{\theta_{CO}^{max}} - \frac{\theta_O}{\theta_O^{max}} \right)^2 ; & 1 - \frac{\theta_{CO}}{\theta_{CO}^{max}} - \frac{\theta_O}{\theta_O^{max}} \geq 0 \\ \\ 0; & 1 - \frac{\theta_{CO}}{\theta_{CO}^{max}} - \frac{\theta_O}{\theta_O^{max}} < 0 \end{cases} . \qquad (8)$$

S_{CO}^0 and $S_{O_2}^0$ are the initial (i.e., at zero coverage) sticking coefficients of CO and O_2, respectively. We will use $S_{CO}^0 = 0.96 (\forall T_s)$ and $S_{O_2}^0 = 0.78 - 7.4 \times 10^{-4} T_s$, where T_s is the sample temperature.[30] For the maximum coverages, we assume $\theta_{CO}^{max} = 0.5$ and $\theta_O^{max} = 0.25$. Those values correspond to the saturation coverages on Pd(111) at $T_s \geq 300$ K.[62]

It should be noted that we have chosen simple (not always realistic) Langmuir's Laws for the sticking coefficients. The only correction concerns the influence of preadsorbed oxygen on sticking of CO [$C_{T_s}(\theta_O / \theta_O^{max})$, Eq. (7)]. It has early been recognized that there is no strong inhibiting effect of preadsorbed oxygen on the sticking coefficient of CO on Pd(111).[29] However, to account for the reaction rate at high oxygen coverage and, therefore, to produce a qualitatively correct transient behavior upon impingement of the CO beam on the oxygen saturated sample, this minor effect has to be taken into account. Erikson and Ekedahl[63] and Piccolo et al.[43] have described the inhibiting effect of oxygen introducing a temperature dependent coefficient C_{T_s} [see Eq. (7)], which is physically related to the presence of a precursor to CO chemisorption. Over the limited temperature range in this study, we have neglected its moderate temperature dependence and have chosen $C_{T_s} = 0.3$ to fit the experimental transient behavior in Fig. 5. Note that the exact choice of this parameter is not of relevance with respect to the following semiquantitative discussion.

In the case of the present experiments, the initial conditions (i.e., just before switching on the CO beam) are $\theta_{CO}(t = t_{CO,on}) = 0$ and $\theta_O(t = t_{CO,on}) = \theta_O^{max} = 0.25$. Besides, step 1 [Eq. (3)] no longer exists at $t > t_{CO,off}$. Thus, the adsorption term in Eq. (7) disappears during this period. The rate constants of the four steps are
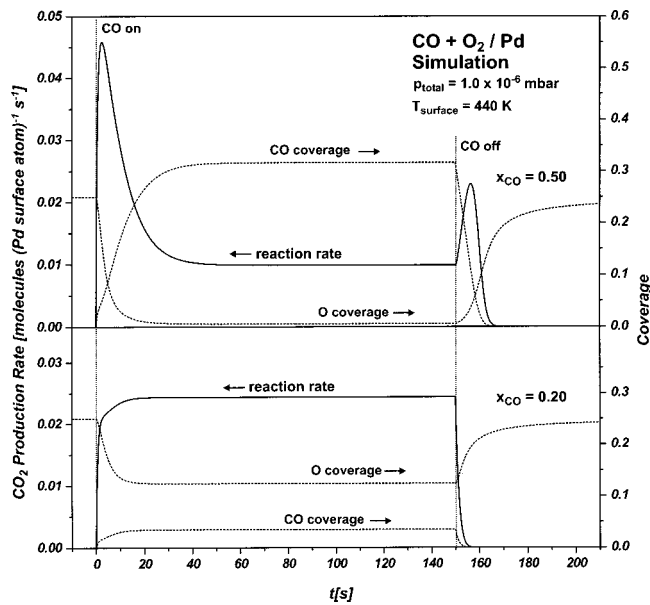
FIG. 11. Simulated transient behavior of the CO_2 production rate, the CO coverage and the oxygen coverage for oxygen rich (bottom trace $x_{CO}=0.2$) and CO rich (top trace, $x_{CO}=0.5$) reaction conditions ($T_{Sample}=440$ K, $p_{total}=1.0\times10^{-6}$ mbar).

$$k_1=\frac{F_{CO}}{n_{Pd}}, \tag{9}$$

$$k_2=v_2\exp\left(\frac{-E_2}{k_BT_s}\right), \tag{10}$$

$$k_3=\frac{F_{O_2}}{n_{Pd}}, \tag{11}$$

$$k_4=v_4\exp\left(\frac{-E_4}{k_BT_s}\right). \tag{12}$$

n_{Pd} is the surface density of Pd atoms on a (111) face: $n_{Pd}=1.53\times10^{15}$ cm^{-2} s^{-1}. v_i and E_i are the frequency factor and the activation energy related to step i, respectively. On the basis of the available literature, these values have been chosen as $v_2=10^{15.0}$ s^{-1}, $E_2=136$ kJ/mol, $v_4=10^{7.9}$ s^{-1}, and $E_4=60$ kJ/mol. Engel and Ertl have determined $E_4=59$ kJ/mol (Ref. 29) for the oxidation step at high coverage and $v_2=10^{14.4\pm0.8}$ s^{-1} and $E_2=134\pm8$ kJ mol^{-1} for the CO desorption on Pd(111).[30] For the model system used here, we have recently measured $v_2=10^{14.9\pm0.9}$ s^{-1} and $E_2=136\pm9$ kJ mol^{-1} for the CO desorption (see Sec. III A) and $v_4=10^{7.0\pm1.0}$ s^{-1} and $E_4=62\pm8$ kJ/mol at low reaction temperatures and high oxygen and moderate CO coverages.[36,40]

Numerical integration of Eqs. (7) and (8) allows us to derive the temporal evolution of CO and O coverages. The CO_2 production rate is then given by

$$r_{CO_2}=k_4\theta_{CO}\theta_O. \tag{13}$$

Results of such calculations for typical reaction conditions ($T_{sample}=440$ K, $p_{total}=1.0\times10^{-6}$ mbar) are plotted in Figs. 11 and 12. As an example, we display the two principle types of transients, i.e., under oxygen-rich conditions (Fig. 11, lower trace, $x_{CO}=0.2$, transient type 1) and under CO-rich conditions (Fig. 11, upper trace, $x_{CO}=0.5$, transient type 2). The additional traces in Fig. 11 represent the CO and O coverages. A comparison with the experimental data in Figs. 3, 5, and 13 shows that the main features of the shape of the experimental reaction rate curve are well reproduced. In particular, the initial CO_2 peak (after CO beam switch-on) and the second CO_2 peak (after CO beam switch-off) under CO rich conditions are well described in a semiquantitative manner. A close comparison with the transient in Fig. 13 recorded under roughly the same conditions (second curve
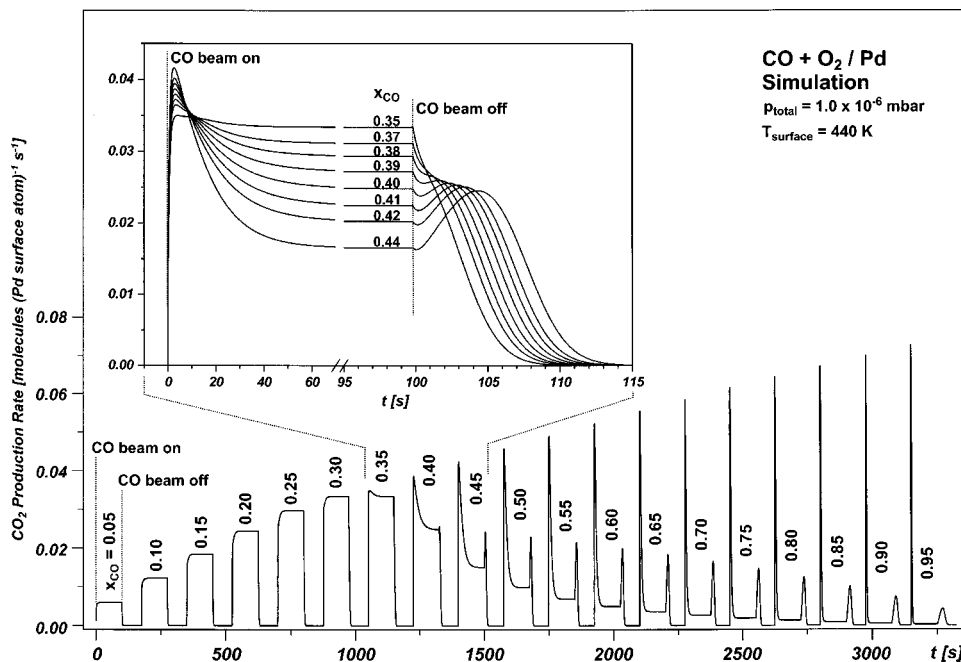

FIG. 12. Simulated transient behavior of the CO_2 production rate as a function of the CO fraction in the impinging gas flux x_{CO} ($T_{Sample}=440$ K, $p_{total}=1.0\times10^{-6}$ mbar). The inset shows the transient behavior in the transition region between the oxygen rich and the CO rich reaction regime.
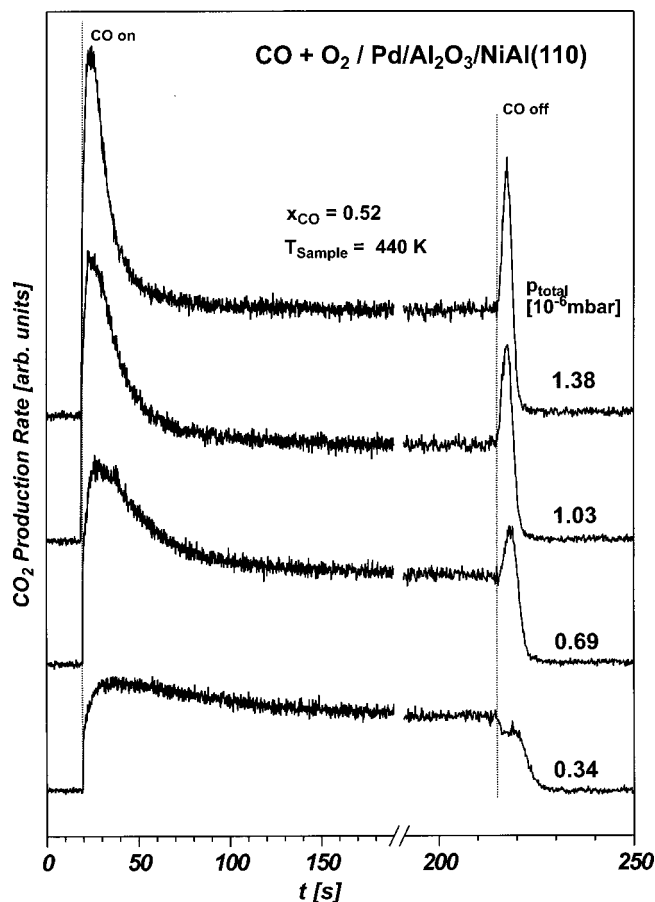
FIG. 13. Transient behavior of the CO_2 production rate as a function of the effective total pressure p_{total}, close to the transition between the two reaction regimes ($T_{Sample} = 415$ K).

from top, $T_{Sample} = 440$ K, $p_{total} = 1.03 \times 10^{-6}$ mbar, $x_{CO} = 0.52$) reveals slight deviations with respect to the shape and the width of both peaks.

In general, these deviations can be considered to be a consequence of the simplistic kinetic model: (a) The exact coverage dependence of both the CO and O_2 sticking coefficients is not taken into account, e.g., the complex influence of precursor states of Ref. 43, (b) the coverage-dependency of energy barriers is not considered, and (c) any influence of the microscopic arrangement of the adsorbates (islanding, etc.) is completely neglected (see, e.g., Ref. 64). Additionally, we disregard all heterogeneity effects, which may exist on the supported model catalyst. Again, it must be underlined that our purpose is not to fit the experimental data, but to explore to what extend the kinetics can be qualitatively explained by a simple homogeneous surface model. It has to be pointed out that considering the present lack of detailed and quantitative information on the reaction system, any further fit of the many parameter system, in particular introducing more complex adsorption and reaction kinetics, does not appear reasonable.

From the transient behavior of the calculated coverages of CO and oxygen (Fig. 11), the first CO_2 peak is easily explained by the fact that, in the considered excess-CO regime (at steady state), the initially higher oxygen coverage and lower CO coverage (as compared to the steady state) are

favorable for the reaction. The same phenomenon can explain the second CO_2 peak: when the CO beam is closed, CO depletion occurs due to reaction or desorption. Subsequently, the adsorption rate of O_2 molecules increases, which results in a transient maximum of the CO_2 production. When no more CO is adsorbed, the CO_2 peak vanishes. This peak can only be observed in the CO-rich regime, where the dissociative chemisorption of O_2 is inhibited by chemisorbed CO.

In Fig. 12, a simulated series of CO_2 transients is shown, for the same reaction conditions as the ones used in the experiment of Fig. 5 ($T_{Sample} = 440$ K, $p_{total} = 1.0 \times 10^{-6}$ mbar). Considering the simplicity of the model, the agreement between the experiment and the simulation is surprisingly good. The oxygen-rich regime (corresponding to the absence of any CO_2 peak during the experiment, i.e., to transients of type 1, see Fig. 3) is present until $x_{CO} \approx 0.35$. The CO-rich regime (corresponding to the presence of a CO_2 peak during the closed-beam period, i.e., to transients of type 2) is reached from $x_{CO} \gtrsim 0.45$.

In the inset in Fig. 12 we consider the transient behavior in the transition region between the oxygen-rich and the CO-rich regime in detail. It is noteworthy that upon termination of the CO beam, a behavior is found which is qualitatively similar to the effect discussed in the previous section. Over a small regime of x_{CO} values between 0.39 and 0.44 we find a sudden decrease of the CO_2 production followed by a peak in the CO_2 production. This subtle effect is a consequence of the competition between two contributions: On the one hand, the reaction rate immediately decreases due to the decreasing CO coverage upon termination of the beam. On the other hand, the oxygen adsorption rate increases due to the decreasing CO coverage. Due to the different kinetics of both processes, the product of the coverages might reach a maximum, giving rise to the CO_2 peak at later time. Although the transient behavior is qualitatively reproduced, some discrepancies remain, comparing the simulation in Fig. 12 with the experimental results shown in Fig. 9. In general, the CO_2 production dip in the simulations appears less pronounced than in the experiment. Similar to the discussion above, the discrepancy may be partially related to the simplifications of the kinetic model. Additionally, the influence of the system heterogeneity may result in an enhancement of this kinetic effect. This will be discussed in detail in Sec. III H.

Finally, we have simulated the experiments of Fig. 6, concerning the steady-state reaction rate at various flux ratios and sample temperatures (for $p_{total} = 1.0 \times 10^{-6}$ mbar). As seen in Fig. 14, the result of such a simulation is again qualitatively satisfying. The general shapes of the curves, the almost linear increase in the high oxygen coverage region, and the position of the maximum as a function of the surface temperature are rather well reproduced. The main difference is related to the high CO-flux side. Whereas the inhibiting effect of CO is reasonably well described for a surface temperature of 440 K, the inhibition is overestimated for lower surface temperatures and underestimated for higher temperatures. To a great extent, this is a consequence of the fact that the current model disregards coverage dependencies of the CO adsorption energy and thus overestimates the CO desorption rate at high temperature and underestimates desorption
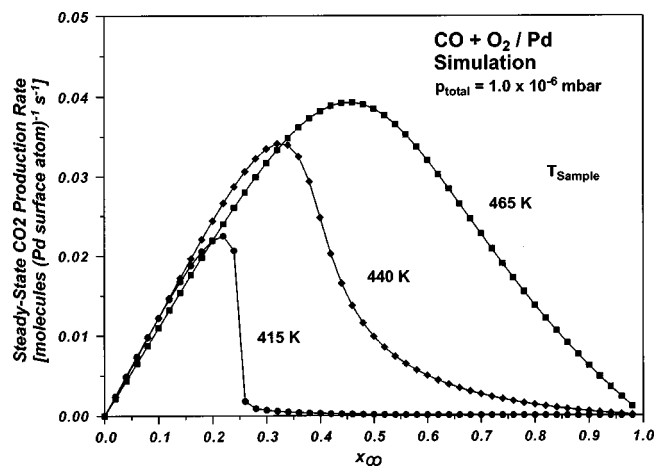
FIG. 14. Simulated steady-state CO_2 production rate as a function of the CO fraction in the impinging gas flux x_{CO} ($p_{total} = 1.0 \times 10^6$ mbar).

at low temperature. On a supported model catalyst, this effect may be particularly relevant due to the variety of available adsorption sites and thus the wider range of adsorption energies.

In conclusion of this section, simple kinetic calculations, assuming a homogeneous surface, and using only a limited set of parameters issuing from literature data, allow to simulate the experiments with a good semiquantitative agreement. The behavior of the transient and steady-state rates as a function of the gas partial pressures and of the surface temperature is well described. In particular, with regard to the transition region between the oxygen and CO rich reaction regimes, it is demonstrated that all the features—including the transient CO_2 production peak—are semiquantitatively reproduced by the homogeneous surface model.

A more quantitative agreement would require a refinement of the simulations, e.g., (a) keeping the ''mean-field'' approach, to improve the model, by using, e.g., coverage-dependent energy barriers for the CO desorption and the CO+O elementary reaction and more realistic sticking coefficients of CO and O_2, or (b) using a more local approach, to account for the fact that the surface of a supported model catalyst is heterogeneous and that the adsorbates are not equally distributed over the sample surface. As a basis, for such an attempt, a detailed knowledge of the energetics and kinetics of the surface–gas interaction and structural characteristics of the catalytic system is required, which is, however, only partially available at present.

H. Discussion

In the previous section we have shown that the transient and steady-state kinetics can at least be semiquantitatively understood assuming a simple homogeneous surface. However, certain deviations remain, in particular with respect to the transient CO_2 peaks. In this final section we will end with a brief discussion, considering how the transient behavior may be further modified by the heterogeneity of the model system.

In general we have to distinguish between intraparticle heterogeneity (different sites or facets on a particle) and in-

terparticle heterogeneity (structural differences between individual particles). In the first case, strong coupling between these sites by surface diffusion has to be taken into account.[5] In the latter case every metal particle represents a largely isolated reaction system. Due to the weak adsorption of the reactants on the alumina support inter-particle diffusion is strongly suppressed. Yet, individual adsorption and the reaction rates on the individual particles may differ considerably, e.g., due to differences in particle size, shape or structure. As a consequence, different steady-state coverages may coexist under given conditions on the individual particles. This effect will be particularly important close to the transition region between the two reaction regimes, where the surface coverages sensitively depend on the reaction parameters. Finally, the total macroscopic reaction rate will be a superposition of the individual particle rates, i.e., a superposition of transients ranging from type 1 (oxygen rich, Fig. 3) to type 2 (CO rich, Fig. 3). As a consequence, we expect that in agreement with the experimental data the characteristic transient CO_2 production in the transition region will occur over a wider range of CO fluxes x_{CO} and may appear more pronounced.

On a microscopic level, there are several pathways via which the heterogeneity of the system may have an influence on the adsorption and reaction rates:

(a) *Variations of the local effective pressure:* At low reaction temperatures a large fraction of the adsorbing reactants is captured via trapping on the support and diffusion to the metal particles. This ''capture zone'' effect has been early discussed by Gillet *et al.*[65] and Henry *et al.*[66] It has been quantitatively investigated in several studies (see, e.g., Refs. 34, 38, 67, 68), recently also on the model system used in this work.[69] This new adsorption channel gives rise to the effect that the reactant flux per Pd surface atom depends on both the particle size and its surrounding. Due to overlapping of the capture zones, on a particle in close proximity to other particles the effective local pressure will be significantly lower than on an isolated particle. This effect is schematically illustrated in Fig. 15. Experimentally, the effect of the total effective pressure p_{eff} at constant x_{CO} is demonstrated in Fig. 13. With increasing total pressure the transient behavior changes in a way similar to what is found for an increasing CO flux fraction at constant total pressure, i.e., with increasing pressure the transition region in a reactivity diagram shifts towards lower CO flux fraction.

(b) *Variations in the sticking coefficient* due to variations in the surface and defect structure.

(c) *Variations in the desorption rate* on different adsorption sites (facets, edges, defects).

(d) *Variations in the reaction rate:* Every particle represents an ensemble of active sites with locally varying activation barriers. Thus the total reaction rate on the particle depends on the ensemble of individual reaction sites.

It remains the question in how far these contributions can be included in further microkinetic simulations to finally

J. Chem. Phys., Vol. 114, No. 10, 8 March 2001

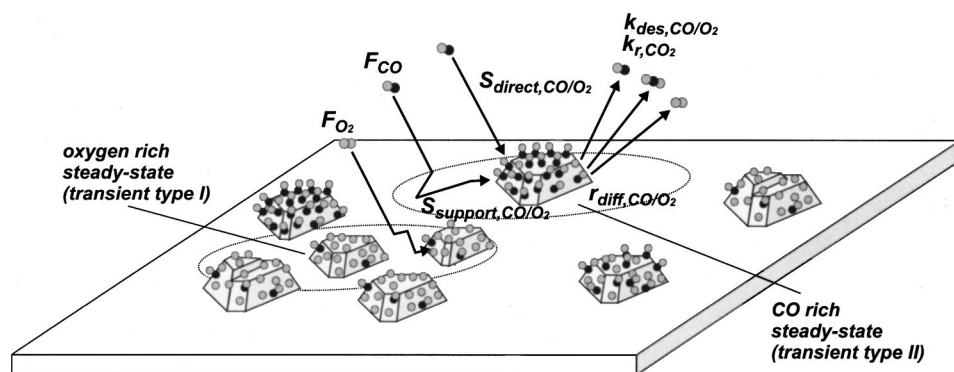CO oxidation kinetics on supported Pd   4683

FIG. 15. Schematic representation of the surface coverages close to the transition region between the oxygen-rich and the CO-region. Depending on their structure and surrounding, some particles may remain in the oxygen-rich state, whereas others switch to the high CO coverage region.

yield a more complete picture of the reaction kinetics on the model system. On complex catalytic surfaces, on which naturally a certain degree of heterogeneity exists, such simulations will finally be necessary in order to identify and quantify the kinetic effects under discussion. As a basis, such simulations, however, require a detailed knowledge of the energetic and structural properties of the model systems. Here, the available data is still rather limited. Whereas some detailed and representative structural information is available from STM and TEM (transmission electron microscopy), the data basis on gas–surface interaction and surface adsorption/ reactions is largely restricted to single-component systems and to ideal single crystal surfaces. Starting from these simple cases, studies on supported model catalysts with a reduced and controllable level of complexity may provide way to address these questions.

IV. CONCLUSIONS

In conclusion, we have applied a combined molecular beam/*in situ* IR reflection absorption spectroscopy approach to study the kinetics of the CO oxidation reaction under steady state and transient conditions. We employ a supported Pd model catalyst, based on an ordered Al_2O_3 film grown on NiAl(110). Previously, this systems has been characterized with respect to its structural and adsorption properties. The surface of the Pd islands is to a large extend dominated by (111)-facets. The particles are characterized by an average size of 5.5 nm and an island density of $10^{12} cm^{-2}$.

(i)   In the temperature range (415–465 K) and pressure range ($\leqslant 10^{-6}$ mbar) investigated, we find no indications for a significant deactivation of the model catalyst on the time scale of the experiment ($\sim 10^3$ s).

(ii)   The steady-state reaction rate was systematically determined as a function of the CO flux fraction and the surface temperature. The different reaction regimes are discussed.

(iii) We have employed *in situ* IRA spectroscopy to follow changes in the occupation of adsorption sites under reaction conditions. Starting from O-rich reaction conditions, the linear increase in CO coverage with the CO flux is accompanied by a increased occupation of bridge sites versus hollow sites, which are predominantly occupied at low CO coverage. The vibrational frequencies are shifted due to the influence of coadsorbed oxygen. In the transition region to the CO-rich regime, the sudden increase in the CO coverage is due to a strongly increased occupation of bridge sites. Additionally, in the high CO-flux region, a small fraction of on-top sites is occupied which may tentatively be assigned to defects.

(iv)   We have systematically investigated the transient behavior of the system under conditions of continuous O_2 flux and modulated CO flux. The different types of transients are discussed. In particular we have investigated the appearance of a transient CO_2 peak after switching off the CO beam. Using time-resolved IR absorption spectroscopy we demonstrate that the observed transient behavior close to the transition region—at least for the model system used in this study—is not related to defect sites, as was proposed previously. Instead we suggest complementary explanations, which are related to (a) the CO induced inhibition of O_2 adsorption and (b) the intrinsic heterogeneity of the model system allowing coexistence of different steady states.

(v)   With a simple kinetic model based on the Langmuir-Hinshelwood mechanism and on previous experimental data available on Pd(111) and on the Pd model system used here, we show that a large part of the reaction kinetics can be understood by considering a homogeneous surface. The good semiquantitative agreement between experiments and simulations is obtained over the range of flux and temperature conditions covered in this study. A close investigation of the CO_2 production after closing of the CO beam suggests, that the transient behavior can be largely explained by these simulations, taking into account the interplay between CO desorption/reaction and the inhibition of O_2 adsorption by CO. Additionally, the effect is expected to be enhanced by the surface heterogeneity of the supported cluster system leading to coexistence of a multitude of differing steady states under given reaction conditions.

[1] M. G. Mason, Phys. Rev. B **27**, 748 (1983).

[2] G. K. Wertheim, Z. Phys. D: At., Mol. Clusters **12**, 319 (1989).

[3] C. R. Henry, C. Chapon, C. Goyhenex, and R. Monot, Surf. Sci. **272**, 283 (1992).

[4] C. R. Henry, Surf. Sci. Rep. **31**, 231 (1998).

[5] V. P. Zhdanov and B. Kasemo, Surf. Sci. Rep. **39**, 25 (2000).

[6] V. P. Zhdanov and B. Kasemo, Surf. Sci. **405**, 27 (1998).

[7] V. P. Zhdanov and B. Kasemo, J. Catal. **170**, 377 (1997).

[8] K. Hayek, R. Kramer, and Z. Paál, Appl. Catal., A **162**, 1 (1997).

[9] S. Ogawa and S. Ichikawa, Phys. Rev. B **51**, 17231 (1995).

[10] G. Rupprechter, G. Seeber, H. Goller, and K. Hayek, J. Catal. **186**, 201 (1999).

[11] G. Pacchioni and N. Rösch, Surf. Sci. **306**, 169 (1994).

[12] G. M. Pajonk, in *Handbook of Heterogeneous Catalysis*, edited by G. Ertl, H. Knözinger, and J. Weitkamp (VCH, Weinheim, 1997), Vol. 3.

[13] W. C. Conner and J. L. Falconer, Chem. Rev. **95**, 759 (1995).

[14] D. W. Goodman, Surf. Rev. Lett. **2**, 9 (1995).

[15] H.-J. Freund, M. Bäumer, and H. Kuhlenbeck, Adv. Catal. **45**, 333 (2000).

[16] M. Bäumer, J. Libuda, A. Sandell *et al.*, Ber. Bunsenges. Phys. Chem. **99**, 1381 (1995).

[17] M. Bäumer, J. Libuda, and H.-J. Freund, in *Chemisorption and Reactivity on Supported Clusters and Thin Films*, edited by M. Lambert and G. Pacchioni (Kluwer Academic, New York, 1997), p. 61.

[18] D. R. Rainer and D. W. Goodman, J. Mol. Catal. A: Chem. **131**, 259 (1998).

[19] H.-J. Freund, Angew. Chem. Int. Ed. Engl. **36**, 452 (1997).

[20] R. M. Jaeger, H. Kuhlenbeck, H.-J. Freund *et al.*, Surf. Sci. **259**, 235 (1991).

[21] J. Libuda, F. Winkelmann, M. Bäumer *et al.*, Surf. Sci. **318**, 61 (1994).

[22] M. Bäumer and H.-J. Freund, Prog. Surf. Sci. **61**, 127 (1999).

[23] K. Wolter, O. Seiferth, H. Kuhlenbeck *et al.*, Surf. Sci. **399**, 190 (1998).

[24] K. H. Hansen, T. Worren, S. Stempel *et al.*, Phys. Rev. Lett. **83**, 4120 (1999).

[25] M. Asscher and G. A. Somorjai, in *Atomic and Molecular Beam Methods*, edited by G. Scoles (Oxford University Press, Oxford, 1988), Vol. 2, p. 489.

[26] M. P. D'Evelyn and R. J. Madix, Surf. Sci. Rep. **3**, 413 (1984).

[27] C. T. Rettner, D. J. Auerbach, J. C. Tully, and A. W. Kleyn, J. Phys. Chem. **100**, 13021 (1996).

[28] J. A. Barker and D. J. Auerbach, Surf. Sci. Rep. **4**, 1 (1985).

[29] T. Engel and G. Ertl, J. Chem. Phys. **69**, 1267 (1978).

[30] T. Engel, J. Chem. Phys. **69**, 373 (1978).

[31] C. T. Campbell, G. Ertl, H. Kuipers, and J. Segner, J. Chem. Phys. **73**, 5862 (1980).

[32] L. S. Brown and S. J. Sibener, J. Chem. Phys. **90**, 2807 (1989).

[33] L. S. Brown and S. J. Sibener, J. Chem. Phys. **89**, 1163 (1988).

[34] I. Stará, V. Nehasil, and V. Matolín, Surf. Sci. **365**, 69 (1996).

[35] I. Stará, V. Nehasil, and V. Matolín, Surf. Sci. **331–333**, 173 (1995).

[36] I. Meusel, J. Hoffmann, J. Hartmann *et al.*, Catal. Lett. (submitted).

[37] C. Becker and C. R. Henry, Catal. Lett. **43**, 55 (1997).

[38] C. Becker and C. R. Henry, Surf. Sci. **352**, 457 (1996).

[39] J. Libuda, I. Meusel, J. Hartmann, and H.-J. Freund, Rev. Sci. Instrum. **71**, 4395 (2000).

[40] I. Meusel, M. Heemeier, B. Richter *et al.* (in preparation).

[41] J. Hoffmann, I. Meusel, J. Hartmann *et al.* (in preparation).

[42] L. Piccolo, Ph.D. thesis, Marseille, 1999.

[43] L. Piccolo, C. Becker, and C. R. Henry, Appl. Surf. Sci. **164**, 156 (2000).

[44] T. Engel and G. Ertl, in *The Chemical Physics of Solid Surfaces and Heterogeneous Catalysis*, edited by D. A. King and D. P. Woodruff (Elsevier, New York, 1982), Vol. 4, p. 73.

[45] H. Graoui, S. Giorgio, and C. R. Henry, Surf. Sci. **417**, 350 (1998).

[46] V. Matolín, E. Gillet, and N. Kruse, Surf. Sci. **186**, L541 (1987).

[47] A. Hammoudeh, Ph.D. thesis, Berlin, 1994.

[48] A. Ortega, F. M. Hoffman, and A. M. Bradshaw, Surf. Sci. **119**, 79 (1982).

[49] A. M. Bradshaw and F. M. Hoffman, Surf. Sci. **72**, 513 (1978).

[50] J. C. Cook, S. K. Clowes, and E. M. McCash, J. Chem. Soc., Faraday Trans. **93**, 2315 (1997).

[51] M. Tüshaus, W. Berndt, H. Conrad *et al.*, Appl. Phys. A: Solids Surf. **51**, 91 (1990).

[52] M. Tüshaus, Ph.D. thesis, Berlin, 1990.

[53] B. Bourguignon, S. Carrez, B. Dragnea, and H. Dubost, Surf. Sci. **418**, 171 (1998).

[54] R. Raval, S. Haq, M. A. Harrison *et al.*, Chem. Phys. Lett. **167**, 391 (1990).

[55] R. Raval, S. Haq, G. Blyholder, and D. A. King, J. Electron Spectrosc. Relat. Phenom. **54-55**, 629 (1990).

[56] H. Pfnür, D. Menzel, F. M. Hoffmann *et al.*, Surf. Sci. **93**, 431 (1980).

[57] L.-W. H. Leung, J. W. He, and D. W. Goodman, J. Chem. Phys. **93**, 8328 (1990).

[58] A. M. deJong and J. W. Niemantsverdriet, J. Chem. Phys. **101**, 10126 (1994).

[59] F. M. Hoffmann, Surf. Sci. Rep. **3**, 107 (1983).

[60] L. Piccolo, C. Becker, and C. R. Henry, Eur. Phys. J. D **9**, 415 (1999).

[61] C. R. Henry, C. Chapon, and C. Duriez, Z. Phys. D: At., Mol. Clusters **19**, 347 (1991).

[62] H. Conrad, G. Ertl, and J. Küppers, Surf. Sci. **76**, 323 (1978).

[63] M. Eriksson and L.-G. Ekedahl, Surf. Sci. **412/413**, 430 (1998).

[64] J. Wintterlin, S. Völkening, T. V. W. Janssens *et al.*, Science **278**, 1931 (1997).

[65] E. Gillet, S. Channakhone, V. Matolin, and M. Gillet, Surf. Sci. **152/153**, 603 (1985).

[66] C. R. Henry and C. Chapon, Surf. Sci. **156**, 952 (1985).

[67] F. Rumpf, H. Poppa, and M. Boudart, Langmuir **4**, 723 (1988).

[68] C. R. Henry, C. Chapon, and C. Duriez, J. Chem. Phys. **95**, 804 (1991).

[69] T. Dellwig, J. Hartmann, J. Libuda *et al.*, J. Mol. Catal. (in press).